Creep on seismogenic faults: Insights from analogue earthquake experiments

Matthias Rosenau*, Michael Rudolf and Onno Oncken

Helmholtz Centre Potsdam, German Research Centre for Geosciences (GFZ), Telegrafenberg, 14473 Potsdam (Germany)

* *rosen@gfz-potsdam.de*

Pre-print in EarthArXiv

Please cite as:

Rosenau, M., Rudolf, and Oncken, O. (2019): Creep on seismogenic faults: Insights from analogue earthquake experiments, EarthArXiv, https://dx.doi.org/10.31223/osf.io/24u5h

https://eartharxiv.org/24u5h

Highlights

- Stick-slip experiments mimic seismogenic fault behavior
- Creep and earthquakes are not mutually exclusive fault styles
- Interseismic creep varies systematically with fault properties and stress state

Keywords

friction, faults, granular materials, aseismic creep, earthquakes, precursors

Abstract

Tectonic faults display a range of slip behaviors including continuous and episodic slip covering rates of more than 10 orders of magnitude (<mm/a to >m/s). The physical control of such kinematic observations remains ambiguous. To gain insight into the slip behavior of brittle faults we performed laboratory stick-slip experiments using a rock analogue, granular material. We realized conditions under which our seismogenic fault analogue shows a variety of slip behaviors ranging from slow, quasi continuous creep to episodic slow slip to dynamic rupture controlled by a limited number of parameters. We explore a wide parameter space by varying loading rate from those corresponding to interseismic to postseismic rates and normal loads equivalent to hydrostatic to lithostatic conditions at seismogenic depth. The experiments demonstrate that significant interseismic creep and earthquakes may not be mutually exclusive phenomena and that creep signals vary systematically with the fault's seismic potential. Accordingly, the transience of interseismic creep scales with fault strength and seismic coupling as well as with the maturity of the seismic cycle. Loading rate independence of creep signals suggests that mechanical properties of faults (e.g. seismic coupling) can be inferred from shortterm observations (e.g. aftershock sequences). Moreover, we observe the number and size of small episodic slip events to systematically increase towards the end of the seismic cycle providing an observable proxy of the relative shear stress state on seismogenic faults. Modelling the data suggest that for very weak faults in a late stage of their seismic cycle, the observed creep systematics may lead to the chimera of a perennially creeping fault releasing stress by continuous creep and/or transient slow slip instead of large earthquakes.

1. Introduction

Faults in the brittle part of the lithosphere may slip at rates ranging from slow, aseismic (< 1 mm/a) to fast, seismic (> 1m/s) (Peng and Gomberg, 2010, and references therein). Moreover they might do so in either continuous (i.e. at constant rate) or transient fashion (at changing rate). Modern geodetic methods allow monitoring fault slip rates over time scales long enough to cover a significant part of the loading history (generally decades) for some fast loading settings like plate boundaries thereby constraining their kinematic behavior with unprecedented resolution (Moreno et al., 2010; Shirzaei and Bürgmann, 2013). Accordingly, a suite of slip behaviors has been observed ranging from continuous creep (e.g., Bokelman and Kovach, 2003) to transient creep (e.g. precursory and afterslip) (e.g. Bedford et al., 2013, Schurr et al., 2014) to episodic slip events at various rates (earthquakes, slow slip and non-volcanic tremor, low frequency earthquakes, creep events) (e.g. Rogers and Dragert, 2003; Ide et al., 2007). High fluid pressure has been identified as a controlling factor for slow slip phenomena (e.g., Peng and Gomberg, 2010, Moreno et al, 2014) but the underlying mechanisms and mechanics controlling which slip behavior prevails remain under determined. Importantly the physics of such faulting is often intrinsically undeterminable in nature because of the inaccessibility of the source and the ambiguity of the geophysical and kinematic observation which can be fitted by more than one theoretical models and/or set of model parameters.

Seismic and aseismic slip behavior are conventually viewed as mutually exclusive at a given location through time. Typically “ambivalent” fault slip behaviors are modelled as a result of the interaction of spatially separated sources, e.g. a seismogenic patch (asperity) embedded in an aseismic area (barriers) (e.g., Wei et al., 2013). However, a more integrative view of slow and fast slip phenomena might be possible where the

slip behavior is non-unique (e.g. Peng and Gomberg, 2010). Indeed, there is recent evidence from longterm geodetic observations as well as contrasting geodetic-seismological versus palaeoseismological observations that given fault areas might be more variable in their slip behaviors than conventionally believed. In particular we now have to acknowledge that a particular fault area may show aseismic creep or slow slip at one time while failing catastrophically in dynamic earthquake ruptures at others. Examples of spatially overlapping seismic and aseismic fault areas have been found along the Hayward fault in California U.S. (Lienkaemper at al., 2012, Shirzaei and Bürgmann, 2013) as well along the subduction megathrusts off Japan (Loveless and Meade, 2011, Kato et al, 2012) and Chile (Moreno et al, 2010, Ruiz et al, 2014). As a reaction to such evidence for non-unique slip behavior, existing friction laws have been adapted for example by allowing aseismic creep at low slip rates but dynamic weakening at high slip rates, e.g. in the presence of fluids (e.g. Noda and Lapusta, 2013).

We here contribute to the discussion of creep signals by means of experimental modeling seismogenic fault slip behavior using a labscale fault analogue under conditions relevant to natural faulting. We show that few parameters can control the rate and stability of fault slip and demonstrate that creeping faults can generate earthquakes. Showing the systematics by which this happens allows inferring information on the mechanical properties and state of the fault from kinematic observations.

2. Friction regimes

The most established view on the mechanics of faulting in the brittle regime (< c. 350°C) is represented by the rate-and-state dependent friction law (e.g. Scholz, 1998). This law opens avenues to explain fault slip behavior over a range of rates. In

particular, it relates aseismic and seismic fault behavior to an intrinsic velocity-strengthening and velocity-weakening fault property, respectively. Accordingly, once static friction is overcome a velocity-weakening fault may weaken dynamically as slip accelerates resulting in a runaway effect or instability and nucleating an earthquake. In contrast, an increase of dynamic friction along a velocity strengthening fault inhibits earthquake nucleation at all times. Importantly, a third regime exists, in which most of the natural faults might actually be, which is characterized by velocity weakening under sufficiently low effective normal stress σ_n' (e.g. near the surface or at high pore fluid pressures). In this regime, which is called the conditionally stable regime, fault slip is slow and stable under quasi-static loading while it can become unstable under dynamic loading (acceleration). "Sufficiently" low effective normal stress in the context of conditional stability means that the externally applied normal load minus the local pore fluid pressure is below a critical value σ_c:

$$\sigma_n' < \sigma_c = kL / -(a-b) \qquad \text{(i)}$$

where k is the spring stiffness in the original theoretical spring slider framework (or the stiffness of the medium in which the fault is embedded), a the instantaneous change of friction following a loading rate change (so-called direct velocity effect) and b the new steady state friction (so-called evolutionary effect) after the loading rate change which evolves over the characteristic slip distance L (a physical interpretation is the size of asperities). The combined parameter a-b is negative for velocity weakening interfaces and positive for velocity-strengthening interfaces. Its absolute values are typically measured in the lab to be in the order of few percent for rocks and other materials (Scholz, 1998; and references therein).

3. Analogue earthquake experimental setup

The laboratory-scale analogue earthquake experiments presented here have been performed in a ring shear tester setup (RST, Figure 1) where a granular material (dry rice) is sheared rotary in a velocity stepping test under imposed normal loads while shear stress is measured continuously (e.g. Rosenau et al., 2017, Rudolf et al., 2019). The rate of laboratory fault slip has been inferred from displacement records derived by particle image velocimetry (PIV, LaVision Strainmaster ®). For PIV analysis, a 12 bit monochrome charged-coupled device (CCD) camera shot sequential images of the analogue fault through a transparent shear cell at a frequency of 10 Hz. The particle motions between successive images are then determined by cross-correlation of textural differences (i.e., gray values) formed by groups of particles within interrogation windows using a Fast Fourier Transform algorithm (Adam et al. 2003). Precision and accuracy of the PIV method is better than 0.1 px of the original image which scales to the order of micrometer in the presented setup.

The stiffness of the loading system (~1.3 kN/mm) together with a-b (~-0.015) and L (~ 2 μm) for dry rice (Rosenau et al., 2009) predicts a critical (effective) normal stress of σ_c = 8 kPa. Accordingly, we performed the tests at 1 – 16 kPa normal load to explore the slip behavior of natural faults across the bifurcation. We refer to the high (8, 16 kPa) and low (1, 2, 4 kPa) normal stress experiments as strong and weak faults, respectively.

Similarity of the experimental simulation with its natural prototype is ensured by keeping the following dimensionless numbers the same: (1) the friction coefficient (ratio between yield strength and normal stress) μ ~0.7, (Byerlee, 1978) and (2) a friction rate parameter a-b ~ -0.015 similar to rocks (e.g., Scholz, 1998) as well as (3)

a dimensionless stress drop (ratio between rupture slip and length) of $\Delta\tau^* \sim 10^{-5} – 10^{-4}$ similar to earthquakes (e.g., Scholz, 1989).

Applying a stress scale of 1:10.000, the setup generates slip instabilities (aka "analogue earthquakes", Figure 2) with stress drops which scale to 1 – 100 MPa in nature typical of large intra- and interplate earthquakes (Scholz, 1989; Hardebeck and Aron, 2009) including precursory events of different scale (Figure 3). The strength of the laboratory fault analogues can be interpreted in two way: Either representing (A) different crustal depths at a given pore fluid pressure (i.e. weak = shallow, strong = deep) or (B) representing different pore fluid pressures at a given depth. For example, at typical seismogenic crustal depths of 5 – 15 km and typical rock densities of 2300 – 2700 kg/m³, the experimental normal stresses (10 – 160 MPa) would correspond to pore fluid pressures of 38 – 96 % lithostatic pressure, i.e. from hydrostatic to near lithostatic. Time is not explicitly scaled in the experiments but imposed loading rates cover more than two orders of magnitude (0.1 – 25 mm/min) similar to post- and interseismic deformation rates in nature (mm/day – mm/year) in order to test possible time scale dependencies (or independencies) of creep signals.

4. Experimental observations and analysis

Analogue fault slip in our experiments is characterized by quasi-periodic stress drops (Figure 2). Quasi-periodic stress drops are preceded by smaller, episodic events (Figure 3). The sizes and recurrence intervals of periodic stress drops are systematically related to the applied normal load and loading rate (Figure 4). This observation is consistent with normal load and loading rate both determining the yield strength according to rate-and-state friction theory (Scholz, 1998). A regular stick-slip behavior is consistent with a characteristic earthquake model where episodic slip occurs at a certain stress level determined by the yield strength and causes relaxation

to a certain lower stress level determined by the residual friction and the stiffness of the loading system.

Beside periodic and episodic stress drops, representing slip during earthquakes and slow slip events, a significant amount of long-term laboratory fault slip occurs as transient creep (accelerating stable slip) between episodic failures. This stable slip during the “stick”-phase causes the stress curves in Figures 2 and 3 to deviate from a linear, elastic loading path. Instead of an ideal “saw tooth” pattern characterizing stress histories of perfect stick-slip, a “shark fin” pattern emerges for the observed stick-creep-slip. In the experiments, up to 80 % of long-term fault slip might be taken up by creep at low effective normal stresses resulting in seismic coupling coefficients (the ratio of seismic to total fault slip) of <0.2 for very weak faults (Figure 2C). At high normal stresses, seismic coupling increases to >0.8 for strong faults in the experiments.

Detailed inspection of the stress loading paths (Figure 5 A) and interseismic creep signals (Figure 5 B) and their time-derivates (i.e. loading and slip rates, Figure 5 C and D) sheds light on the time and stress dependencies of laboratory fault creep. Accordingly, stress in the inter-event time (which is normalized to a unit interval here) accumulates in a more transient, non-linear fashion for weak faults than it does for strong faults (red versus blue curves in Figure 5 A and C). Strong faults show a stressing rate which is almost consistent with elastic loading except prior to an event (i.e. runs parallel long-term rate in Figure 5 C) while stressing rates of weak faults vary by more than an order of magnitude. Slip varies consistently with loading. Accordingly, slip accumulates in a more non-linear for strong faults than it does for weak faults (Figure 5 B) covering two orders of magnitude in slip rate versus less than one, respectively (Figure 5 D).

Connecting stress and strain allow us to describe the creep behavior of our fault analogues as follows: Creep along strong laboratory faults accelerates at rather constant stressing rate late in the interseismic period leading to episodic failure ("precursory slip"). Weak faults instead creep at higher rates throughout the interseismic period but more continuously and at progressively decreasing stressing rate. Moreover, strong faults reach only about half of the long-term fault slip rate towards the very end of the loading cycle, whereas weak faults may creep at almost the long-term rate for the second half of the loading cycle.

In order to analyze the creep behavior systematically as controlled by extrinsic factors (normal stress and loading rate) we attempted to quantify the non-linearity (or transience) of stress and slip accumulation by a single, dimensionless parameter. Therefore we calculated the area beneath the normalized stress and strain accumulation curves in Figure 5 A and B, respectively, which we call the unit stress and unit strain integrals (Figure 5E). Clearly, these measures of transience decrease systematically with increasing applied normal stress or fault strength as expected from the observations before. However, they do not correlate with loading rate, an observation that is not intuitive but useful as will be discussed below. The positive correlation between the unit stress and slip integrals (Figure 5F) indicates the consistency of our independent stress and stain observations and is a direct result of the intrinsic velocity weakening behavior of the laboratory fault.

Irrespective of fault strength, episodic slip events of various speeds occur at high stress level modulating the interseismic creep signal in the late stage of the analogue seismic cycle (Figure 3). Preliminary analysis suggests that these precursor events increase systematically in number and size as the fault evolves towards failure.

5. Discussion

5.1 Inversion of fault properties and state from creep signals

The observation of continuous and transient creep signals as well as episodic slow slips which are systematically linked to fault properties and maturity of the loading cycle or stress level but independent of loading rate bear important implications for the interpretation of fault creep records as observable proxies for fault strength and seismic potential. Fault creep records in nature are generally short with respect to the seismic cycle. The results obtained here suggest that any creep record, though only a snapshot of the full seismic cycle, might bear important information on long-term fault properties and hazardous behavior.

Using the analog fault observations from the here presented experiments, an empirical inversion scheme as proposed in Figure 6 can be applied, where inaccessible fault properties like fault strength, seismic coupling, stress drop and recurrence interval can be inferred from the observable transience of interseismic creep signals. Here, creep transience (CT) is defined as

$$CT = 2 \cdot (1 - 2 \cdot \text{unit slip integral}) \qquad \text{(ii)}$$

in order to derive a dimensionless (and therefore scale-independent) parameter which varies between 0 (linear strain accumulation) and 1 (non-linear, highly transient strain accumulation).

Linear regression analysis of the experimentally derived data plotted in such a scheme indicates a significant correlation between creep signals and fault properties and behavior but independence of loading rate. More specifically, fault strength, seismic coupling, stress drop as well as recurrence period show a positive linear or log-linear dependency with CT ($R^2 > 0.6 – 0.8$).

Importantly, no significant correlations exist between any of the parameters with loading rate. This is indicated by the rather horizontal or scattered distribution of data from subsets with the same fault strength measured at different velocities in Figure 6 as well as the collapse of time-series data from such subsets in Figure 5. The fact that the systematics found experimentally are loading rate independent suggest that short-term observations can be extrapolated to larger earthquakes and longer recurrence intervals. I.e. this timescale independency opens the opportunity to generalize fault properties or behavior derived during aftershocks sequences or earthquake swarms or from repeating events to longterm (multiple seismic cycles) fault behavior.

An observation not quantified in detail here is the occurrence of precursor slip events of different scale and velocity which systematically increase in number and size towards the end of a seismic cycle (Figure 3). Several large earthquakes in subduction zones have actually been preceded by accelerating foreshock activity (e.g. Bouchon et al., 2013). Especially the recent 2014 8.1 Pisagua earthquake offshore Chile showed accelerating foreshock activity with a decrease in b-value (representing an increase in the number of large events relative to small events) over the decade preceding the main shock (Schurr et al., 2014). If such a systematic behavior can be generalized and physically explained it should lead to a better ability to forecast earthquakes.

5.2 Revisiting creep records along the San Andreas Fault

In order to test and apply our proposed inversion scheme, we use the longest creep records available and revisit the San Andreas Fault data. California creepmeters have been installed across the San Andreas Fault in the late 1960s (Schulz et al., 1982), geodetic surveys took place since the mid-1970s (Burford and Harsh, 1980; Lisowski and Prescott, 1981) and surface velocities from space-geodetic measurements are available since about a decade (e.g., Bürgmann et al., 2000; Titus et al., 2006). For a

mean recurrence interval of large Californian earthquakes of about 150 ± 50 years along any SAF segment (e.g. Zielke et al., 2010), the observation time frame generally represents less than half of the seismic cycle length. Nevertheless, the records are probably the best data we can get today.

Seismic and aseismic strike-slip along the central SAF (cSAF) accounts for most of the Pacific-Great Valley microplate relative motion in central California (Thatcher, 1979; Lisowski and Prescot, 1981, Titus et al., 2006; Rolandone et al., 2008; Ryder and Bürgmann, 2008). As suggested by over 40 years of creep and earthquake records, the central section of the cSAF creeps continuously at a decadal scale at about 28 mm/a at seismogenic depth (0 – 12 km, Schulz et al., 1982, Titus et al., 2006, Rolandone et al., 2008). This long-term creep is modulated by shorter term transients presumably very shallow (< 5 km) and related to earthquakes (Lisowski and Prescott, 1981; Thurber, 1996). At seismogenic depths repeating microearthquakes occur (Nadeau and McEvilly, 2004) indicating that locally and/or transiently, velocity weakening behavior is established along the fault. Noticeably, the current creep of cSAF is only about 80 – 90 % of the far-field, tectonic loading rate (31 – 35 mm/a, Titus et al., 2006, Rolandone et al., 2008; Ryder and Bürgmann, 2008) suggesting a slip deficit of few millimeter accumulating each year. Right-lateral shear strains in the sidewalls of the cSAF are evidently very small (Rolandone et al., 2008, Savage, 2009) suggesting a small stressing rate. Episodic slow slip events as they occur late in the interseismic period in our experiments (Figure 3) have been reported as potential earthquake pre-cursors along the SAF by Thurber (1996) and Thurber and Sessions (1998) based on temporal cross-correlation of creepmeter records and seismological catalogues. Though the correlations they found were statistically significant, the feedback mechanism remained unclear. Noticeably, they did not find a clear spatial

299 relation between the loci of creep and earthquakes which would be required by our
300 model. Moreover, they assigned creep to the very shallow crust (<5 km) and not to
301 seimogenic depths. Whilst the adjoining segments ruptured in large earthquakes in
302 1906 (San Francisco) and 1857 (Fort Tejon), the creeping section of the cSAF has not
303 experienced large earthquakes in the historic past (~300 years).

304 In the light of the experiments done in this study the key question is: Does the absence
305 of large earthquakes, the high and continuous creep rates as well as the low shear
306 strain accumulation serves as a good indicator that this fault segment poses no seismic
307 hazard?

308 Applying the empirical inversion scheme established above (Figure 6), we would
309 infer first that the creeping section of the cSAF is a very weak fault based on the
310 rather linear slip accumulation signal (Schulz et al., 1982, Titus et al., 2006) and low
311 stressing rate (Rolandone et al., 2008, Savage, 2009). This is consistent with previous
312 findings based on the observation of low resolved shear stresses along the creeping
313 section and absence of a heat flow anomaly (Brune et al., 1969, Lachenbruch and
314 Sass, 1980, Zoback et al., 1987).

315 The cSAF shows therefore kinematic similarity to our weak fault analogue
316 characterized dynamically by low seismic coupling and small stress drops during
317 earthquakes. This may however not mean that the seismic potential is low. In contrast:
318 Because stress drop is only a weak measure of earthquake size, which scales
319 dominantly with the rupture area, and because low seismic coupling (or vice versa a
320 large amount of interseismic creep) just stretches the recurrence intervals of
321 potentially large earthquakes. We will elaborate on this effect in the next section.

5.3 Modelling the effect of creep on recurrence time and the chimera of perennially creeping faults

Because of the empirically found correlation between fault strength and creep, the net effect of creep on the recurrence interval of earthquakes should not only take into account the stretching of the recurrence interval due to creep but also a modification of recurrence interval due to changes in strengths (Figure 4). Such a scenario is illustrated in Figure 7.

Quantitatively, creep lengthens the (effective) recurrence interval to

$$t^* = 1/(1\text{-creep}). \qquad \text{(iii)}$$

For example a fault where 50 % of longterm slip is accommodated aseismically requires twice as much time to reach a certain stress level again. However, because creep correlates with fault weakness and weaker faults fail at lower stress level in quicker succession for the same far field stressing rate (Figure 4), this lengthening effect is to some degree counterbalanced by shorter recurrence intervals.

In Figure 7 we plot the effective recurrence time observed in our experiments in relation to creep on faults of variable strength and model the data as the combined result of the competing effects of “creep lengthening” (according to eq. (iii)) and “weakness shortening”. The latter effect is taken into account by fitting an exponential relation of the form

$$t^{**}=e^{(-A \times \text{creep})} \qquad \text{(iv)}$$

to the data. Parameter A is an empirically derived proxy for the relation between strength and recurrence interval and varies between 4 and 6 in our example. The net effect of “creep lengthening” and “weakness shortening” of recurrence intervals, i.e. the effective recurrence interval, is then simply

$$t = t^* \times t^{**} = 1/(1-\text{creep})\, e^{(-A \times \text{creep})}. \quad (v)$$

For the parameter space realized in our experiments recurrence time is always shorter than on faults without creep, i.e. the weakness effect dominates the recurrence behavior such that more creeping faults have systematically shorter recurrence times. However, at least theoretically our model predicts for very weak faults (not realized in our experiments) with very low seismic coupling coefficients and very high creep amounts, the lengthening effect should start dominating and consequently the effective recurrence intervals should become longer than without creep. For creep amounts exceeding 98% effective recurrence times may well exceed any historical record for fast creeping faults (Figure 7). In the extreme such a seismically nearly uncoupled, very weak fault appears as seismically silent over many human generations – obviously a chimera.

5.4 Creep on continental vs. subduction megathrusts

Locking pattern of continental and subduction megathrusts show a striking qualitative difference: While continental megathrusts, e.g. the Himalayan main thrust, show homogeneous and high locking with little interseismic creep (Stevens and Avouac, 2015), subduction megathusts, like the Chilean subduction zone, show a patchy locking pattern indicating a significant amount of creep (e.g. Saillard et al., 2017). According to our experiments, and in line with theory, such a qualitative difference can be explained by higher amounts water entrained into subduction megathrust compared to continental settings, lowering the effective normal load and this enhancing creep. However, other explanations exist like differences in lithology and even lack of offshore geodetic coverage.

6 Conclusion

Based on stick-slip experiments using a labscale fault analogue, we explored the slip behavior of seismogenic faults and tested the potential to derive information on fault properties and state from kinematic observables. We showed that the stress buildup between episodic failures (analogue earthquakes) is non-linear and anti-correlated with the creep signals. According to our experiments the transience of stress buildup and creep is controlled primarily by fault normal stress, i.e. related to frictional strength and/or pore-fluid pressure, and systematically reflect the seismic coupling coefficient and maturity of the seismic cycle. Application of these systematics to the creeping section of the central San Andreas fault suggests that this fault branch may not be aseismic on the long term (millennia scale) but is in a late stage of a seismic cycle which exceeds historic records. The qualitative difference in creep on megathrusts between homogenously fully locked continental versus heterogeneously locked subduction megathrusts may be similarly explained by the presence of water in oceanic settings.

Acknowledgements

This study has been partially funded by the German Research Foundation (DFG) collaborative research center SFB1114 “Scaling Cascades in Complex Systems”, project B01.

Figure Captions

Figure 1: Analogue earthquake experimental setup: (A) side (camera) view of the sample (rice) in a transparent shear cell in situ in the ring-shear tester, boundary conditions and observables indicated; PIV velocities are representative of a slip event. (B) sketch of the ring-shear tester setup (modified from Schulze (2003)) with PIV camera position indicated.

Figure 2: Stress and strain time-series of laboratory faults: (A) Stress time series measured during velocity stepping tests under variable normal loads simulating seismic and aseismic slip along very weak to strong fault slip. Note the periodic stress drops representing analogue earthquakes. (B) Slip time series for very weak and strong faults derived by PIV. (C) Variation of seismic coupling over the parameter space tested here. Note the sensitivity of seismic coupling to normal load and insensitivity to loading rate.

Figure 3: Examples of precursory slip events along laboratory faults (from Rosenau et al., 2017): (A) stress time series, (B) Histogram of number of slow slip events per unit interseismic time interval. Note the increase of precursory events in size and number towards the end of the seismic cycle.

Figure 4: Dependency of recurrence interval and stress drop on loading rate and normal load over the parameters space tested here.

Figure 5: Systematics of interseismic stress-strain relationships for laboratory faults: (A) interseismic stress accumulation (normalized), (B) interseismic slip accumulation (normalized), (C) interseismic stress rate (normalized), (D) interseismic slip rate (normalized), (E) Variation of unit stress and slip integrals over the parameter space

tested here, (F) correlation of unit stress and slip integrals indicating velocity weakening behaviour.

Figure 6: Dependency of creep signal transience on laboratory fault properties: (A) fault strength as a function of creep transience, (B) seismic coupling as a function of creep transience, (C) stress drop as a function of creep transience, (D) recurrence period as a function of creep transience.

Figure 7: Modelling the effect of fault creep and strength on recurrence time of earthquakes. Experimental data are fitted by theoretical model taking into account two competing effect: Fault creep lengthens recurrence intervals ("creep lengthening effect") while weakening faults should shorten recurrence intervals ("weakness shortening effect"). The effective recurrence is dominated by the weakness effect for faults creeping up to 98%. However, faults which accumulate >98 % of fault slip aseismically may still generate earthquakes with recurrence periods exceeding historical records (California earthquake history shown as example).

References:

1. Adam, J., O. Oncken, N. Kukowski, J. Lohrmann, S. Hoth, J. L. Urai, W. van der Zee, J. Schmatz, B. Wieneke, and K. Pfeiffer (2005), Shear localisation and strain distribution during tectonic faulting - New insights from granular-flow experiments and high-resolution optical image correlation techniques, Journal of Structural Geology, 27(2), 183-301.
2. Bedford, J., et al. (2013), A high-resolution, time-variable afterslip model for the 2010 Maule Mw=8.8, Chile megathrust earthquake, Earth and Planetary Science Letters, 383, 26-36.
3. Bokelmann, G. H. R. (2003), Long-term creep-rate changes and their causes, Geophysical Research Letters, 30(8).
4. Bouchon, M., V. Durand, D. Marsan, H. Karabulut, and J. Schmittbuhl (2013), The long precursory phase of most large interplate earthquakes, Nature Geoscience, 6(4), 299-302.
5. Brune, J. N., T. L. Henyey, and R. F. Roy (1969), Heat flow, stress, and rate of slip along the San Andreas Fault, California,Journal of Geophysical Research, 74(15), 3821--3827.
6. Burford, R. O., and P. W. Harsh (1980), Slip on the San Andreas fault in central California from alinement array surveys, Bulletin of the Seismological Society of America, 70(4), 1233-1261.
7. Byerlee, J. (1978), Friction of rocks, Pageoph, 116, 615-626.
8. Bürgmann, R., D. Schmidt, R. M. Nadeau, M. d'Alessio, E. Fielding, D. Manaker, T. V. McEvilly, and M. H. Murray (2000), Earthquake Potential

Along the Northern Hayward Fault, California, Science, 289(5482), 1178-1182.

9. Hardebeck, J. L., and A. Aron (2009), Earthquake Stress Drops and Inferred Fault Strength on the Hayward Fault, East San Francisco Bay, California, Bulletin of the Seismological Society of America, 99(3), 1801-1814.

10. Ide, S., G. C. Beroza, D. R. Shelly, and T. Uchide (2007), A scaling law for slow earthquakes, Nature, 447(7140), 76-79.

11. Kato, A., K. Obara, T. Igarashi, H. Tsuruoka, S. Nakagawa, and N. Hirata (2012), Propagation of Slow Slip Leading Up to the 2011 M-w 9.0 Tohoku-Oki Earthquake, Science, 335(6069), 705-708.

12. Lachenbruch, A. H., and J. H. Sass (1980), Heat flow and energetics of the San Andreas Fault Zone, Journal of Geophysical Research: Solid Earth, 85(B11), 6185--6222.

13. Lienkaemper, J. J., J. N. Baldwin, R. Turner, R. R. Sickler, and J. Brown (2013), A Record of Large Earthquakes during the Past Two Millennia on the Southern Green Valley Fault, California, Bulletin of the Seismological Society of America, 103(4), 2386-2403.

14. Lisowski, M., and W. H. Prescott (1981), Short-range distance measurements along the San Andreas fault system in central California, 1975 to 1979, Bulletin of the Seismological Society of America, 71(5), 1607-1624.

15. Loveless, J. P., and B. J. Meade (2011), Spatial correlation of interseismic coupling and coseismic rupture extent of the 2011 MW= 9.0 Tohoku-oki earthquake, Geophysical Research Letters, 38(17).

16. Moreno, M., M. Rosenau, and O. Oncken (2010), 2010 Maule earthquake slip correlates with pre-seismic locking of Andean subduction zone, Nature, 467(7312), 198-202.

17. Moreno, M., C. Haberland, O. Oncken, A. Rietbrock, S. Angiboust, and O. Heidbach (2014), Locking of the Chile subduction zone controlled by fluid pressure before the 2010 earthquake, Nature Geoscience, 7(4), 292-296.

18. Nadeau, R. M., and T. V. McEvilly (2004), Periodic Pulsing of Characteristic Microearthquakes on the San Andreas Fault, Science,303(5655), 220-222.

19. Noda, H., and N. Lapusta (2013), Stable creeping fault segments can become destructive as a result of dynamic weakening,Nature, 493(7433), 518-+.

20. Peng, Z. G., and J. Gomberg (2010), An integrated perspective of the continuum between earthquakes and slow-slip phenomena, Nature Geoscience, 3(9), 599-607.

21. Rogers, G., and H. Dragert (2003), Episodic tremor and slip on the Cascadia subduction zone: The chatter of silent slip, Science,300, 1942-1943.

22. Rolandone, F., R. Bürgmann, D. C. Agnew, I. A. Johanson, D. C. Templeton, M. A. d'Alessio, S. J. Titus, C. DeMets, and B. Tikoff (2008), Aseismic slip and fault-normal strain along the central creeping section of the San Andreas fault, Geophysical Research Letters, 35(14), n/a--n/a.

23. Rosenau, M., J. Lohrmann, and O. Oncken (2009), Shocks in a box: An analogue model of subduction earthquake cycles with application to seismotectonic forearc evolution, Journal of Geophysical Research, 114(B1).

24. Rosenau, M., F. Corbi, S. Dominguez (2017): Analogue earthquakes and seismic cycles: Experimental modelling across timescales, Solid Earth, doi: 10.5194/se-2016-165

25. Rudolf, M., Rosenau, M. , Ziegenhagen T., et al. (2019): Smart speed imaging in Digital Image Correlation: Application to seismotectonic scale modelling, Front. Earth Sci., https://doi.org/10.3389/feart.2018.00248

26. Ruiz, S., M. Metois, A. Fuenzalida, J. Ruiz, F. Leyton, R. Grandin, C. Vigny, R. Madariaga, and J. Campos (2014), Intense foreshocks and a slow slip event preceded the 2014 Iquique Mw 8.1 earthquake, Science.

27. Ryder, I., and R. Bürgmann (2008), Spatial variations in slip deficit on the central San Andreas Fault from InSAR, Geophysical Journal International, 175(3), 837--852.

28. Saillard, M., L. Audin, B. Rousset, J. P. Avouac, M. Chlieh, S. R. Hall, L. Husson, and D. L. Farber (2017), From the seismic cycle to long-term deformation: linking seismic coupling and Quaternary coastal geomorphology along the Andean megathrust, *Tectonics*, 36(2), 241-256.

29. Savage, J. C. (2009), Comment on “Aseismic slip and fault-normal strain along creeping section of the San Andreas Fault” by F. Rolandone et al., Geophysical Research Letters, 36(13), n/a--n/a.

30. Scholz, C. H. (1989), Mechanics of Faulting, Ann. Rev. Earth Planet. Sci., 17, 309-334.

31. Scholz, C. H. (1998), Earthquakes and friction laws, Nature, 391, 37-42.

519 32. Schulze, D. (2003), Time- and velocity-dependent properties of powders
520 effecting slip-stick oscillations, Chemical Engineering & Technology, 26(10),
521 1047-1051.

522 33. Schurr, B., et al. (2014), Gradual unlocking of plate boundary controlled
523 initiation of the 2014 Iquique earthquake, Nature,512(7514), 299-+.

524 34. Shirzaei, M., and R. Buergmann (2013), Time-dependent model of creep on
525 the Hayward fault from joint inversion of 18years of InSAR and surface creep
526 data, Journal of Geophysical Research-Solid Earth, 118(4), 1733-1746.

527 35. Stevens, V.L., Avouac, J.-P. (2015), Interseismic coupling on the main
528 Himalayan thrust. *Geophysical Research Letters*,doi:10.1002/2015GL064845

529 36. Thatcher, W. (1979), Horizontal crustal deformation from historic geodetic
530 measurements in southern California, Journal of Geophysical Research: Solid
531 Earth, 84(B5), 2351--2370.

532 37. Thurber, C. H. (1996), Creep events preceding small to moderate earthquakes
533 on the San Andreas fault, Nature, 380, 425 - 428.

534 38. Titus, S. J., C. DeMets, and B. Tikoff (2006), Thirty-Five-Year Creep Rates
535 for the Creeping Segment of the San Andreas Fault and the Effects of the 2004
536 Parkfield Earthquake: Constraints from Alignment Arrays, Continuous Global
537 Positioning System, and Creepmeters, Bulletin of the Seismological Society of
538 America, 96(4B), S250-S268.

539 39. Wei, M., Y. Kaneko, Y. J. Liu, and J. J. McGuire (2013), Episodic fault creep
540 events in California controlled by shallow frictional heterogeneity, Nature
541 Geoscience, 6(7), 566-570.

40. Zielke, O., J. R. Arrowsmith, L. G. Ludwig, and S. O. Akçiz (2010), Slip in the 1857 and Earlier Large Earthquakes Along the Carrizo Plain, San Andreas Fault, Science, 327(5969), 1119-1122.

41. Zoback, M. D., et al. (1987), New Evidence on the State of Stress of the San Andreas Fault System, Science, 238(4830), 1105-1111.

Figure 1

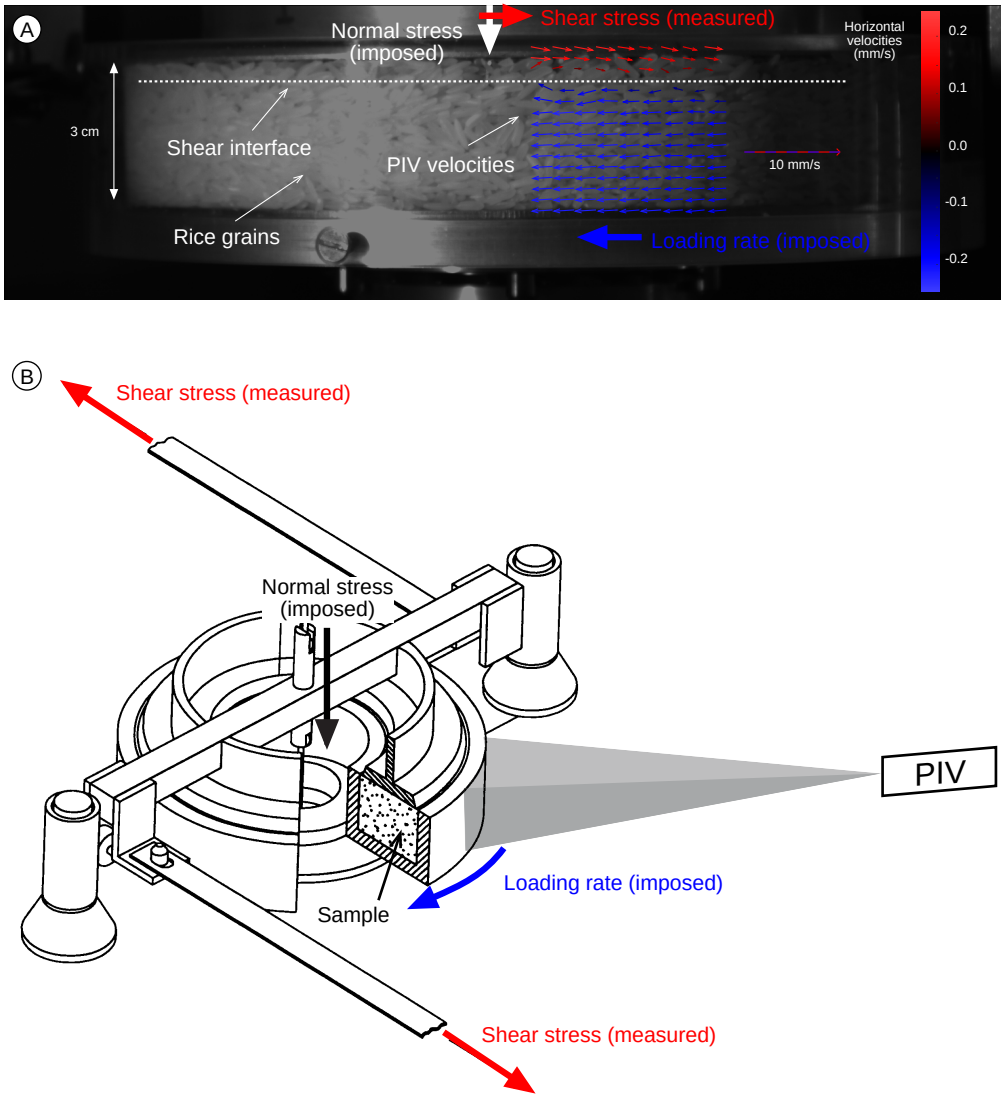
A
Normal stress
(imposed)
Shear stress (measured)
Horizontal
velocities
(mm/s)
0.2
0.1
0.0
-0.1
-0.2
3 cm
Shear interface
PIV velocities
10 mm/s
Rice grains
Loading rate (imposed)
B
Shear stress (measured)
Normal stress
(imposed)
PIV
Loading rate (imposed)
Sample
Shear stress (measured)

Figure 2

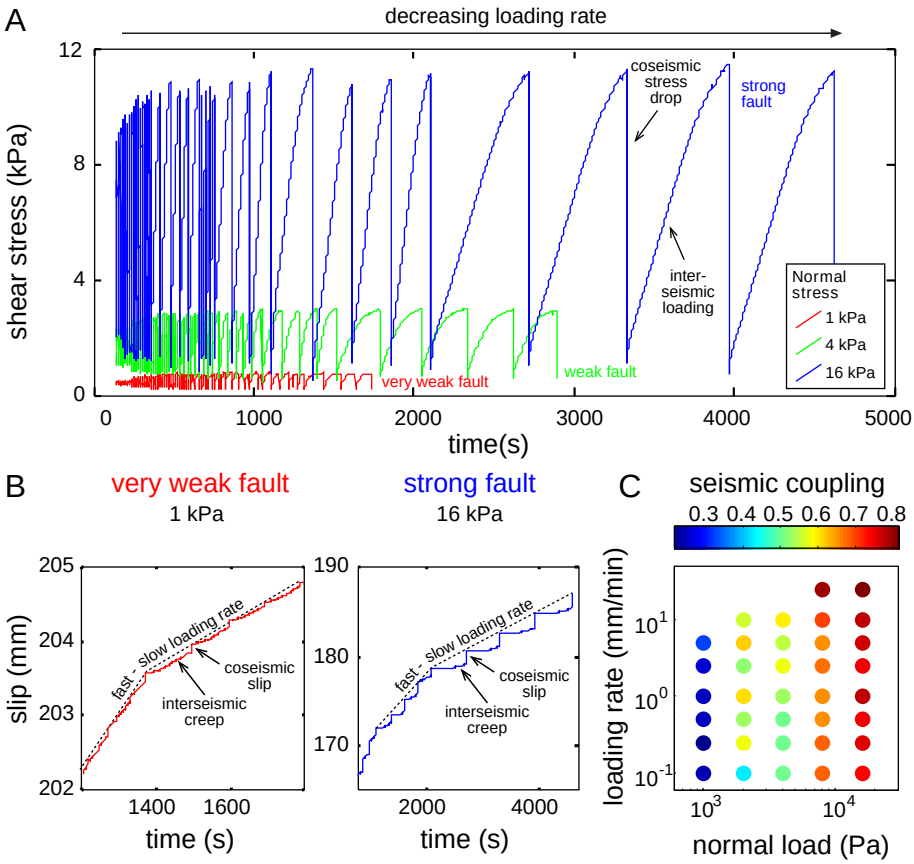
A
decreasing loading rate
shear stress (kPa)
time(s)
coseismic stress drop
strong fault
inter-seismic loading
very weak fault
weak fault
Normal stress
1 kPa
4 kPa
16 kPa
B
very weak fault
1 kPa
strong fault
16 kPa
slip (mm)
fast - slow loading rate
coseismic slip
interseismic creep
time (s)
C
seismic coupling
0.3 0.4 0.5 0.6 0.7 0.8
loading rate (mm/min)
normal load (Pa)

Figure 3

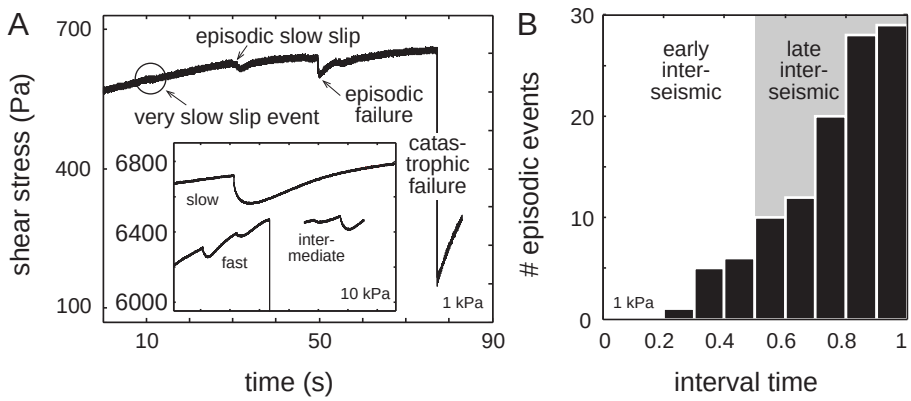
A
700
400
100
shear stress (Pa)
episodic slow slip
very slow slip event
episodic failure
catas-trophic failure
6800
6400
6000
slow
fast
inter-mediate
10 kPa
1 kPa
10
50
90
time (s)
B
30
20
10
0
episodic events
early inter-seismic
late inter-seismic
1 kPa
0
0.2
0.4
0.6
0.8
1
interval time

Figure 4

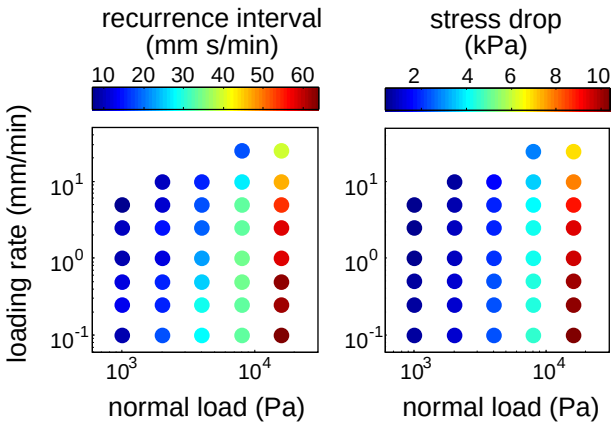
recurrence interval
(mm s/min)
10 20 30 40 50 60
stress drop
(kPa)
2 4 6 8 10
loading rate (mm/min)
10^1
10^0
10^{-1}
10^3
10^4
normal load (Pa)
normal load (Pa)

Figure 5

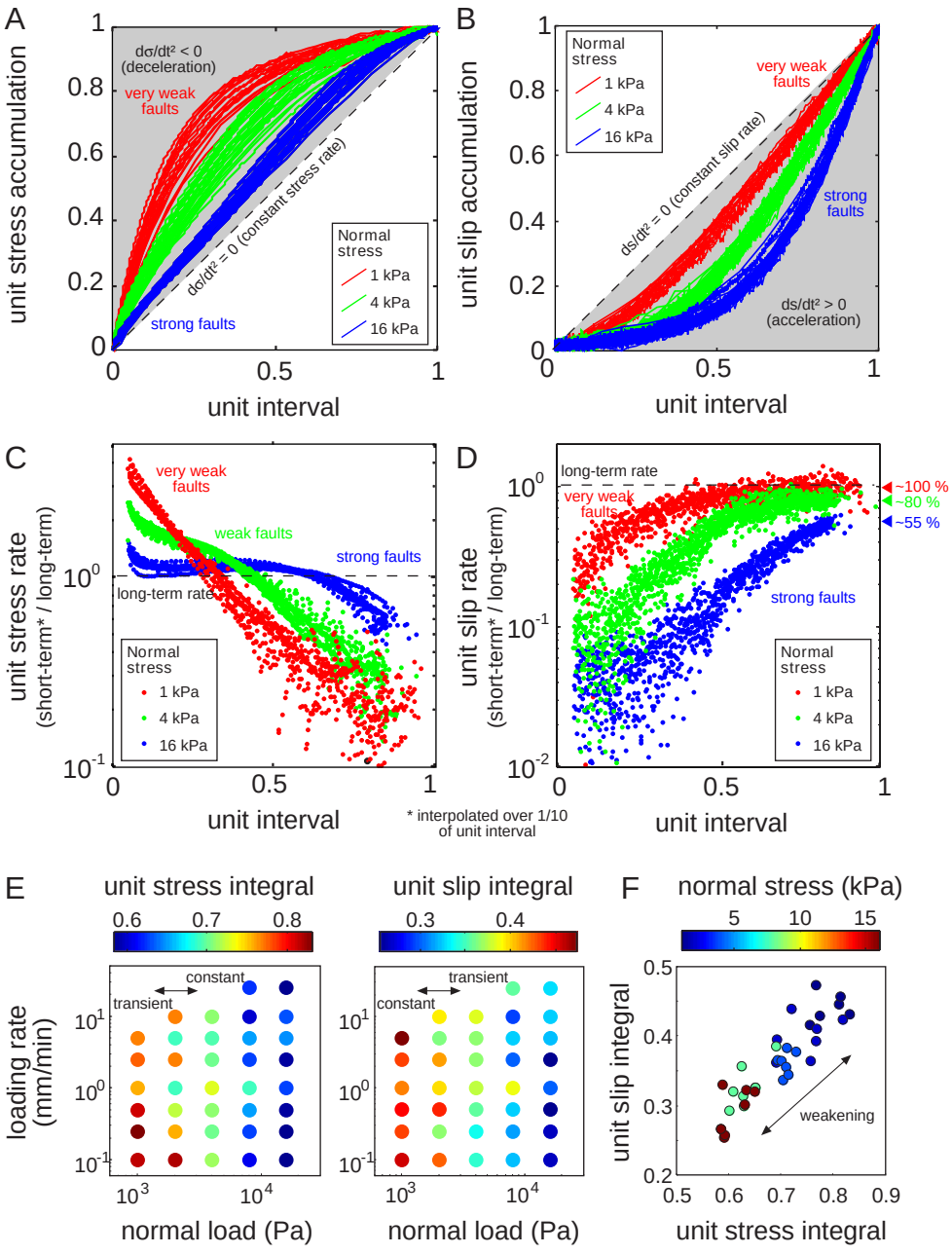
A
unit stress accumulation
dσ/dt² < 0
(deceleration)
very weak
faults
dσ/dt² = 0 (constant stress rate)
strong faults
Normal
stress
1 kPa
4 kPa
16 kPa
unit interval
B
unit slip accumulation
Normal
stress
1 kPa
4 kPa
16 kPa
very weak
faults
ds/dt² = 0 (constant slip rate)
strong
faults
ds/dt² > 0
(acceleration)
unit interval
C
unit stress rate
(short-term* / long-term)
very weak
faults
weak faults
strong faults
long-term rate
Normal
stress
1 kPa
4 kPa
16 kPa
unit interval
* interpolated over 1/10
of unit interval
D
unit slip rate
(short-term* / long-term)
long-term rate
very weak
faults
strong faults
~100 %
~80 %
~55 %
Normal
stress
1 kPa
4 kPa
16 kPa
unit interval
E
unit stress integral
0.6
0.7
0.8
unit slip integral
0.3
0.4
loading rate
(mm/min)
constant
transient
transient
constant
normal load (Pa)
normal load (Pa)
F
normal stress (kPa)
5
10
15
unit slip integral
weakening
unit stress integral

Figure 6

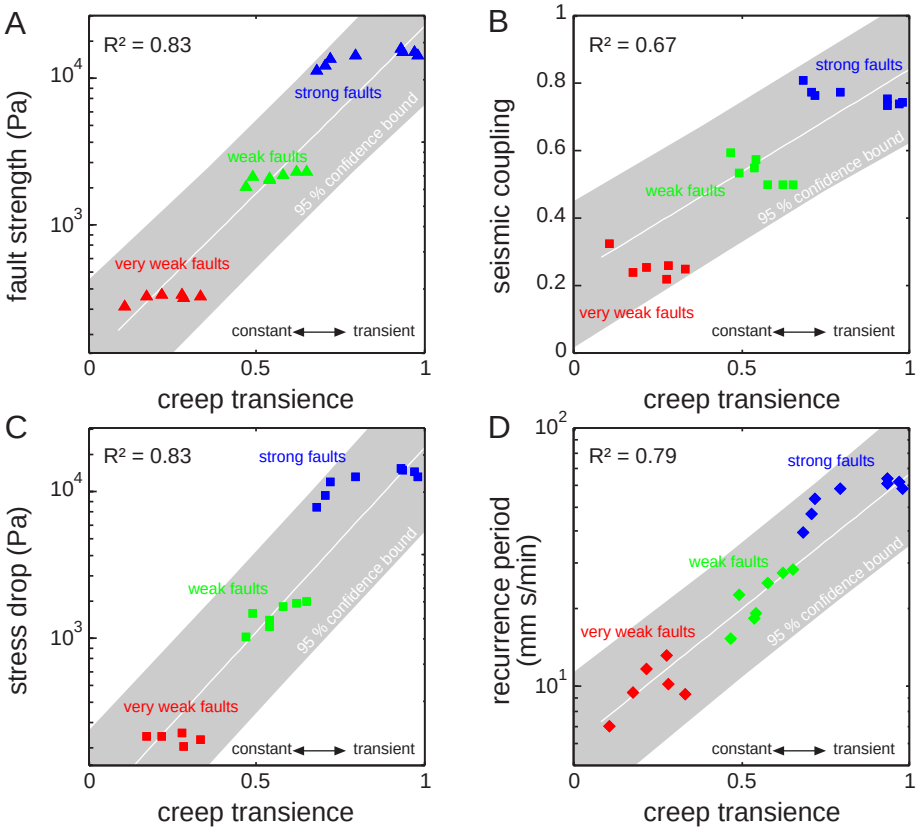
A
R² = 0.83
strong faults
weak faults
very weak faults
95 % confidence bound
constant
transient
fault strength (Pa)
creep transience
B
R² = 0.67
strong faults
weak faults
very weak faults
95 % confidence bound
constant
transient
seismic coupling
creep transience
C
R² = 0.83
strong faults
weak faults
very weak faults
95 % confidence bound
constant
transient
stress drop (Pa)
creep transience
D
R² = 0.79
strong faults
weak faults
very weak faults
95 % confidence bound
constant
transient
recurrence period (mm s/min)
creep transience

Figure 7

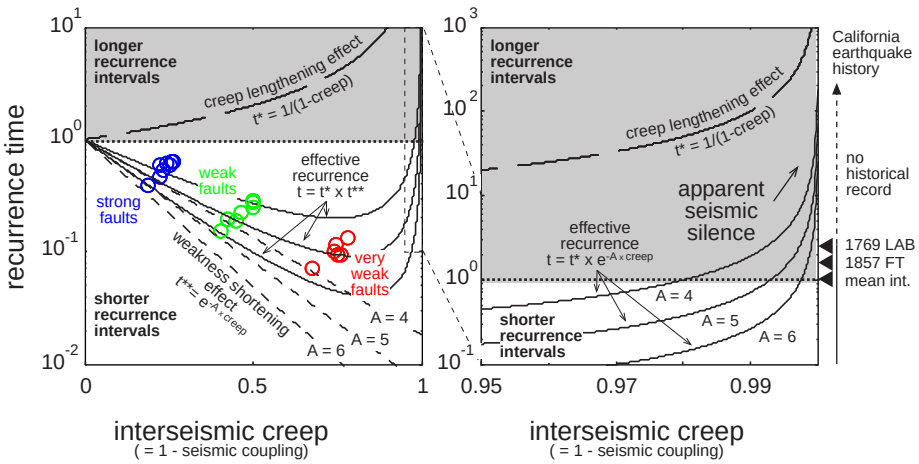
recurrence time
longer recurrence intervals
creep lengthening effect
t* = 1/(1-creep)
weak faults
strong faults
effective recurrence
t = t* x t**
very weak faults
weakness shortening effect
t** = e-A x creep
shorter recurrence intervals
A = 4
A = 5
A = 6
interseismic creep
(= 1 - seismic coupling)
apparent seismic silence
effective recurrence
t = t* x e-A x creep
California earthquake history
no historical record
1769 LAB
1857 FT
mean int.